Lasers in Manufacturing Conference 2021

Welding mode identification using a combination of OCT and photodiode signal

Tobias Beck [a,b,*], Christoph Bantel [a], Meiko Boley [a], Jean Pierre Bergmann [b]

[a] *Corporate Research, Robert Bosch GmbH, Robert-Bosch-Campus 1, 71272 Renningen, Germany*
[b] *Production Technology Group, Technische Universität Ilmenau, Gustav-Kirchhoff-Platz 2, 98693 Ilmenau, Germany*

Abstract

The high absorptivity (~ 40 %) of copper for green laser light, allows for new process zones with a wide and shallow capillary. This can benefit process monitoring while laser beam welding, due to the improved accessibility of the capillary. In this publication, the usage of an OCT system in conjunction with a photodiode to determine the welding mode during copper welding of with green lasers is presented. A good agreement of the OCT depth and weld depth is shown. However, for parameter sets where the welding regime is presumably heat conduction welding, a capillary depth greater than zero was measured. Three different welding modes could be identified as a result: Welding without measured depth and no material evaporation, welding with measurable depth but without material evaporation, and welding with measured depth and material evaporation. In order to identify the welding mode correctly, a photodiode was used to measure the temperature radiation of the welding process. A correlation between the signal characteristic and the presence of material evaporation could be established. By using both sensors in conjunction, it was possible to correctly identify the different welding modes during copper welding with green lasers.

Keywords: copper welding; micro welding; process control; optical coherence tomography; process emissions

1. Introduction

As the consequences of global warming become more apparent, a reduction of carbon emissions is imperative. The efforts to reduce carbon emissions can be supported by future electrification in transport (Gryparis, 2020). As electrification progresses, so does the need for reliable copper joints, for which laser beam welding has become a key technology (Heider, 2019). However, due to the complexity of laser beam welding,

* Corresponding author. Tel.: +49 711 811 13775.
E-mail address: Tobias.Beck2@de.bosch.com.

reliable process monitoring has proven to be difficult (Norman et al., 2007). Especially in power electronics, small weld dimensions and short process times pose additional challenges. By using laser beam sources with shorter wavelengths, the welding process benefits from an increased absorption of the radiation in the material (Engler et al., 2011) compared to state-of-the-art lasers with a wavelength of 1 µm. This allows new process zones to be reached with a stable and shallow capillary, which also benefits process monitoring due to better accessibility of the capillary.

The potential of using a green laser for welding copper could be shown by Alter et al., 2018. In contrast to laser welding with IR laser systems, a smooth increase in the welding depth could be determined during the transition from heat conduction to deep penetration welding. The capillary depth measurement in copper welding using green lasers with an optical coherence (OCT) system was demonstrated by Beck et al., 2021. Interestingly, a depth could be measured during presumably heat conduction welding before transitioning to deep penetration welding. This leads to the conclusion that the sole use of an OCT system to determine the welding regime is not sufficient and thus additional sensor systems are necessary.

Therefore, a combination of two sensor systems - an OCT to determine the depth and a photodiode to detect evaporation - is used to determine the present welding mode.

2. Experimental Setup and Methods

2.1. Material and Optical setup

A schematic of the experimental setup is displayed in Fig. 1. Pure copper samples (Cu-ETP) with dimensions of 40 mm x 20 mm x 2 mm were used. No shielding gas was applied. As the laser source, a green laser with a wavelength of 515 nm (TruDisk Pulse 421, Trumpf) was used. A fibre with a core diameter of 150 µm and lens with a magnification of two was used. This resulted in a focal diameter of 300 µm. The focal position was set on the sample surface. The movement of the processing beam relative to the sample surface was realized by using a galvanometric scanner.

The welding process was observed coaxially using three different diagnostic systems. The capillary depth was measured using an optical coherence system (LDD-600; IPG Photonics) with a measuring wavelength of 840 nm and an acquisition rate of 200 kHz. The focal diameter of the OCT measuring beam of was measured to be ~ 33 nm. To compensate for the displacement of the deepest capillary point with changing process parameters, the position of the OCT beam was offset based on the investigations of Beck et al., 2021.

Additionally, the process was observed using a High-Speed Camera (Phantom VEO 1310, Vision Research) at a framerate of 50 kHz and a resolution of 640 x 240 pixels, which resulted in an observed area of 8000 µm x 3000 µm. The image was filtered by using a short-pass filter with a cut-off wavelength of 750 nm (FESH750, Thorlabs) and a notch filter with a center wavelength of 514±2 nm (NF514-17, Thorlabs) to filter out both the OCT radiation and the processing laser.

Lastly, the temperature radiation of the welding process was observed using an InGaAs photodiode. The temperature radiation was filtered using a long-pass filter with a cut-on wavelength of 900 nm (FELH900, Thorlabs). The signal of the photodiode was recorded by a real time measurement System (ADwin-Pro II, Jäger Computergesteuerte Messtechnik GmbH) with an acquisition rate of 250 kHz.

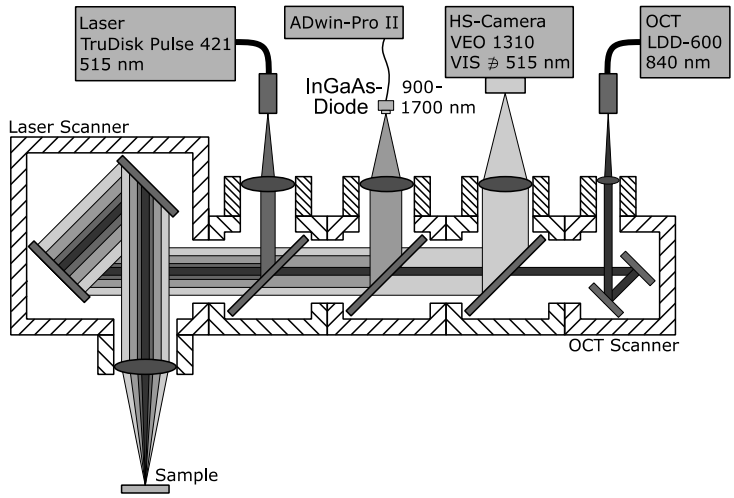

Fig. 1. Schematic of the experimental setup used in the experiments.

In the experiments the laser power as well as the welding speed were varied in-between experiments while the focal diameter remained constant. The welding speed was varied in the range of 250 mm/s up to 750 mm/s while the laser power was varied from 1000 W to 3000 W. Six repetitions were carried out for each process parameter.

2.2. Assessment criteria for the welding regime

The threshold of deep-penetration welding is described by Graf et al., 2015. It is stated that: *"As soon as the intensity is high enough that the melt starts to vaporize near the center of the beam, a small pit is formed in the melt due to the evaporation pressure which further increases the absorbed radiation due to multiple reflections in the pit."*

To determine the welding regime, the images from the coaxial high-speed camera were evaluated. Fig. 2 shows a sequence of high-speed images displaying the change from heat conduction welding to deep penetration welding. From left to right the welding time increases. A significant increase in brightness can be seen between the images at the times of 5.50 ms and 5.52 ms, indicating material evaporation and the transition to the deep-penetration welding regime. In the following, this increase in brightness is used as criterion for deep penetration welding.

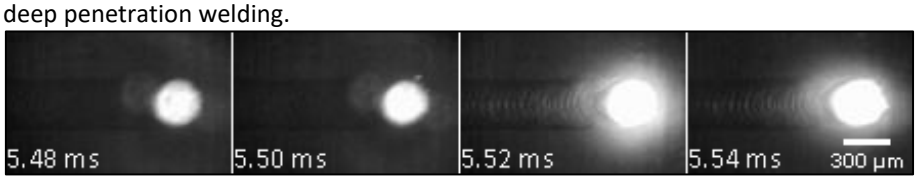

Fig. 2 Sequence of coaxial high-speed images of a welding process transferring from heat conduction welding to deep-penetration welding.

2.3. Evaluation of the temperature radiation

Ramsayer, 2006 has shown that a change of welding modes can be identified in the signal of a photodiode that detects radiation in the range of 1100 nm to 1700 nm. Consequently, the temperature radiation of the

welding process was measured using an InGaAs photodiode in a wavelength range from 900 nm to 1700 nm. The material evaporation changes the signal in such a way, that the Signal-to-noise ratio

$$SNR = \frac{\mu}{\sigma}, \tag{1}$$

where μ is the mean of the recorded signal and σ is the standard deviation, changes drastically. In order to be able to determine presence of material evaporation locally at each point in time, the formula was adapted to calculate a rolling SNR with a window size of 40 µs.

3. Results and discussion

3.1. OCT depth measurement

The results of the OCT measurement (OCT depth) in addition to the real welding depth (weld depth) are shown in Fig. 3 as a function of the laser power. The welding speed can be distinguished by the colour and shape, where cyan pentagons represent a welding speed of $v = 250\,\frac{\text{mm}}{\text{s}}$, blue triangles $v = 500\,\frac{\text{mm}}{\text{s}}$, and red diamonds $v = 750\,\frac{\text{mm}}{\text{s}}$. To distinguish the corresponding measurements, the shapes marking the weld depth are outlined in black. The welding regime determined by the visible material evaporation in the high-speed video is indicated by the background colour, with a grey background representing heat conduction welding and a white background representing deep penetration welding. In addition, the transition area from heat conduction welding to deep penetration welding is displayed as a magnified inlay.

With increasing laser power, an increase in weld depth can be observed, which is also accompanied by an increase in the OCT depth. In contrary, an increase of the welding speed leads to a decrease of both values. During the transition from heat conduction welding to deep penetration welding, a sharp increase in welding and OCT depth is observed at welding speeds of $250\,\frac{\text{mm}}{\text{s}}$ and $500\,\frac{\text{mm}}{\text{s}}$. For a welding speed of $750\,\frac{\text{mm}}{\text{s}}$, a smooth transition with only a small increase in weld depth can be observed. Interestingly, an increase in OCT depth can be also observed during heat conduction welding. At a laser power of 1500 W and a welding speed of $750\,\frac{\text{mm}}{\text{s}}$, a depth of ~ 50 µm was measured. This leads to the assumption that a small pit must have formed during heat conduction welding.

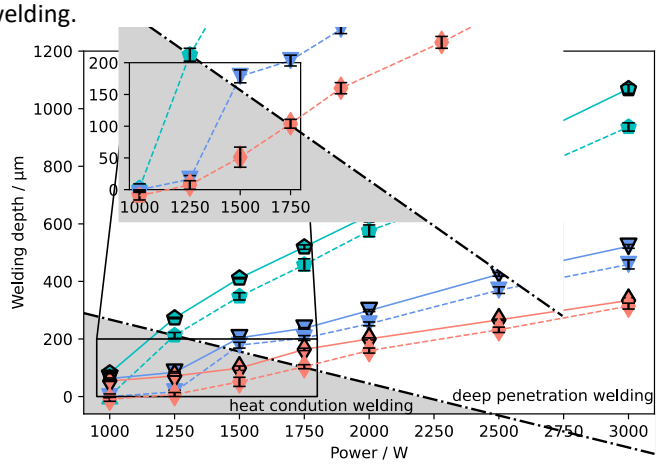

Fig. 3. Mean welding and capillary depth (n=6) as a function of the laser power and welding speed; with outline: welding depth; no outline: capillary depth measurement; grey background: heat conduction welding; white background: deep penetration welding.

Close to the deep penetration threshold, this effect could also be observed for welding speeds of $500\,\frac{mm}{s}$. To illustrate this effect, Fig. 4 shows a weld seam (upper image) that was created using a welding speed of $500\,\frac{mm}{s}$ and a laser power of 1500 W, combined with the corresponding longitudinal section (lower image). Additionally, the weld depth (black) as well as the OCT depth (blue) measurement are marked in the longitudinal section.

In the upper image (top view), a change of colour and overall appearance can be seen approximately in the middle of the weld seam. In the corresponding high-speed video the material evaporation is visible from this point in time. A slight increase weld seam width and weld depth as well as an increase in pore formation can be observed. However, the OCT depth only changes insignificantly.

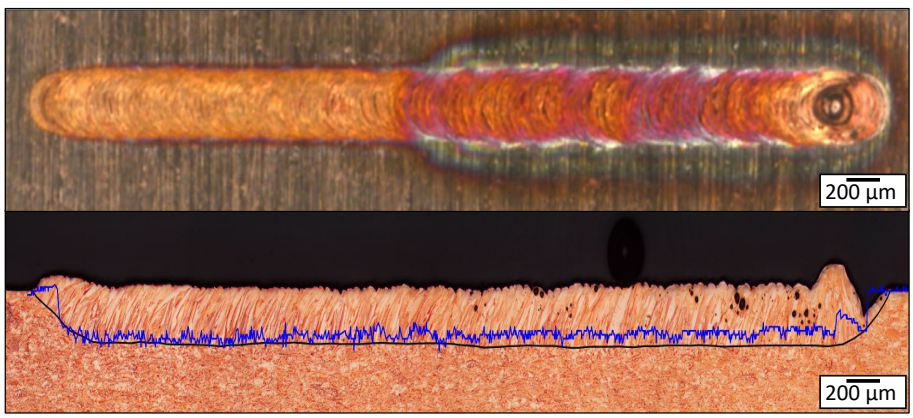

Fig. 4. Weld seam with a corresponding longitudinal cross section for a laser power of 1500 W and a welding speed of $500\,\frac{mm}{s}$.

As a result, three different welding modes can be identified for copper welding with green lasers: welding without measurable depth and material evaporation, welding with a measurable depth and no material evaporation as well as welding with a measured depth and presence of material evaporation. This leads to the conclusion that the sole use of an OCT system is not sufficient to determine the welding mode during copper welding with green lasers. Therefore, an additional sensor is necessary in conjunction with the OCT system to identify the welding mode and will be presented in the following.

3.2. Detection of material evaporation

As mentioned before, the temperature radiation can be used to distinguish between different welding modes. In Fig. 5, the previously shown weld image is shown along with the signal of the temperature radiation. With the onset of material evaporation, which is accompanied by a colour change on the surface, an increased fluctuation of the signal can be observed.

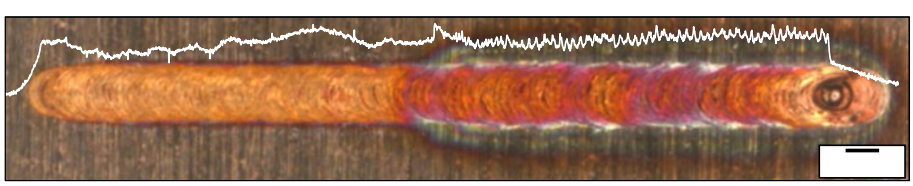

Fig. 5. Weld seam image overlayed with the measured temperature radiation for a laser power of 1500 W and a welding speed of $500\,\frac{mm}{s}$.

Using the presented method in section 2.3, the fluctuation of the signal was evaluated using the signal to noise ratio (SNR). By comparing the determined SNR values to the presence of material evaporation, the usability of the temperature radiation is evaluated. In Fig. 6, the presence of material evaporation visible in the high-speed video is shown as a function of the SNR. Where no evaporation is detected, a high SNR in the range of ~60 to 175 is found, while values below 50 are the case in welding experiments with evaporation.

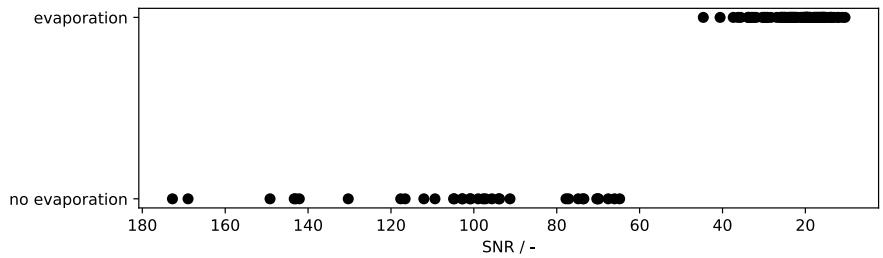

Fig. 6. Presence of evaporation as a function of the determined SNR.

This leads to the conclusion that the temperature radiation can be used in conjunction with the presented method to detect the presence of material evaporation.

3.3. Combination of Sensor Information

In the previous sections, the OCT depth measurement and the material evaporation detection method were presented. In order to identify the different welding modes present in copper welding with green lasers, the use of the individual sensors has proven to be insufficient. However, by combining both sensor information, additional information about the welding process can be derived.

In Fig. 7, the SNR of the temperature radiation is displayed as a function of the OCT depth. The welding mode can be distinguished by colour, with cyan representing a welding mode with no OCT depth and no material evaporation. Red dots represent experiments where an OCT depth could be measured despite the lack of material evaporation, while blue dots represent experiments with a measured OCT depth and the presence of material evaporation. The welding mode is also indicated by the position of the measuring points in the diagram. Measuring points without measured depth and without material evaporation are located in the upper left section. As soon as a depth can be measured, the measuring points shift to the upper right section, while measuring points with measured depth and material evaporation are located in the lower right section.

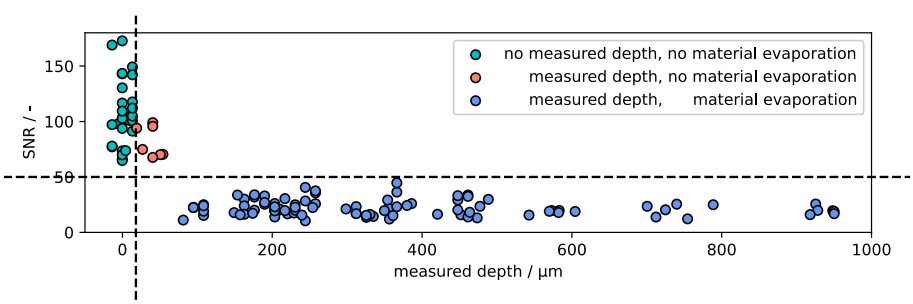

Fig. 7. SNR of the temperature radiation as function of the OCT depth.

In conclusion, by combining the information from both sensor systems, additional information about the process can be derived. The combination of OCT depth measurement and the material evaporation determined through the temperature radiation enabled the correct identification of the current welding mode during copper welding with a green laser, in contrast to the use of individual sensor information.

4. Conclusion

In this publication, the use of an OCT system in combination with a photodiode to determine the welding mode in copper welding with green lasers is presented. A good agreement of the OCT depth and weld depth is shown. However, for parameter sets where the welding regime is presumably heat conduction welding, a capillary depth greater than zero was measured. By evaluating the OCT depth measurement and the high-speed videos, three different welding modes could be identified: welding without measured depth and material evaporation, welding with measurable depth but without material evaporation, and welding with measured depth and material evaporation. To correctly identify the welding mode, the use of the OCT depth alone has proven to be insufficient. In order to additionally determine the material evaporation, the temperature radiation of the process was measured using an InGaAs photodiode. A correlation between the signal fluctuation and the presence of material evaporation could be established. By combining the information from both sensor systems, the OCT depth measurement and the presence of material evaporation, it was possible to correctly identify the different welding modes during copper welding with green lasers.

Acknowledgements

The OCT system was provided by the company PT Photonic Tools GmbH (Björn Wedel). The sponsorship and support is gratefully acknowledged.

References

Alter, L., Heider, A. , Bergmann, J.P., 2018. Investigations on copper welding using a frequency-doubled disk laser and high welding speeds. Procedia CIRP, Elsevier BV, 2018, 74, 12-16.

Beck, T., Bantel, C., Boley, M., Bergmann, J.P., 2021. OCT Capillary Depth Measurement in Copper Micro Welding Using Green Lasers. Appl. Sci. 2021, 11, 2655.

Engler, S., Ramsayer, R. , Poprawe, R., 2011. Process Studies on Laser Welding of Copper with Brilliant Green and Infrared Lasers, Physics Procedia, Elsevier BV, 2011, 12, 339-346.

Graf, T., Berger, P., Weber, R., Hügel, H., Heider, A., Stritt P., 2015. Analytical expressions for the threshold of deep-penetration laser welding. Laser Phys. Lett. 12 (2015) 056002 (5pp).

Gryparis, E., Papadopoulos, P., Leligou, H. C., Psomopoulos, C. S., 2020. Electricity demand and carbon emission in power generation under high penetration of electric vehicles. A European Union perspective. Energy Reports, Elsevier BV, 2020, 6, 475-486.

Heider, A., 2019. Laser Welding Of Copper For E-Mobility Applications - Challenges, Limits And Strategies Using Different Laser Technologies, 8th International Congress on Laser Advanced Material Processing, May 2019.

Norman, P., Engström, H., Kaplan, A., 2007. State-of-the-art of monitoring and imaging of laser welding defects, 11th NOLAMP Conference in Laser Processing of Materials, August, 2007.

Ramsayer, R. M., 2005. Prozessstabilisierung beim gepulsten Laserstrahlmikroschweißen von Kupferwerkstoffen RWTH Aachen, RWTH Aachen.